Patch Complexity, Finite Pixel Correlations and Optimal Denoising

Anat Levin[1], Boaz Nadler[1], Fredo Durand[2], and William T. Freeman[2]

[1] Weizmann Institute
[2] MIT CSAIL

Abstract. Image restoration tasks are ill-posed problems, typically solved with priors. Since the optimal prior is the exact unknown density of natural images, actual priors are only approximate and typically restricted to small patches. This raises several questions: How much may we hope to improve current restoration results with future sophisticated algorithms? And more fundamentally, even with perfect knowledge of natural image statistics, what is the inherent ambiguity of the problem? In addition, since most current methods are limited to finite support patches or kernels, what is the relation between the patch complexity of natural images, patch size, and restoration errors? Focusing on image denoising, we make several contributions. First, in light of computational constraints, we study the relation between denoising gain and sample size requirements in a non parametric approach. We present a law of diminishing return, namely that with increasing patch size, rare patches not only require a much larger dataset, but also gain little from it. This result suggests novel adaptive variable-sized patch schemes for denoising. Second, we study absolute denoising limits, regardless of the algorithm used, and the converge rate to them as a function of patch size. Scale invariance of natural images plays a key role here and implies both a strictly positive lower bound on denoising and a power law convergence. Extrapolating this parametric law gives a ballpark estimate of the best achievable denoising, suggesting that some improvement, although modest, is still possible.

1 Introduction

Characterizing the properties of natural images is critical for computer and human vision [20,13,22,18,6,26]. In particular, low level vision tasks such as denoising, super resolution, deblurring and completion, are fundamentally ill-posed since an infinite number of images x can explain an observed degraded image y. Image priors are crucial in reducing this ambiguity, as even approximate knowledge of the probability $p(x)$ of natural images can rule out unlikely solutions.

This raises several fundamental questions. First, at the most basic level, what is the inherent ambiguity of low level image restoration problems? i.e., can they be solved with zero error given perfect knowledge of the density $p(x)$? More practically, how much can we hope to improve current restoration results with future advances in algorithms and image priors?

Clearly, more accurate priors improve restoration results. However, while most image priors (parametric, non-parametric, learning-based) [2,14,22,18,26] as well as studies on image statistics [13,6] are restricted to local image patches or kernels, little is

A. Fitzgibbon et al. (Eds.): ECCV 2012, Part V, LNCS 7576, pp. 73–86, 2012.

known about their dependence on patch size. Hence another question of practical importance is the following: What is the potential restoration gain from an increase in patch size? and, how is it related to the "patch complexity" of natural images, namely their geometry, density and internal correlations.

In this paper we study these questions in the context of the simplest restoration task: image denoising [20,22,5,10,8,16,9,26]. We build on prior attempts to study the limits of natural image denoising [19,3,7]. In particular, on the non-parametric approach of [14], which estimated the optimal error for the class of patch based algorithms that denoise each pixel using only a finite support of noisy pixels around it. A major limitation of [14], is that computational constraints restricted it to relatively small patches. Thus, [14] was unable to predict the best achievable denoising of algorithms that are allowed to utilize the entire image support. In other words, an absolute PSNR bound, independent of patch size restrictions, is still unknown.

We make several theoretical contributions with practical implications, towards answering these questions. First we consider non-parametric denoising with a finite external database and finite patch size. We study the dependence of denoising error on patch size. Our main result is a *law of diminishing return*: when the window size is increased, the difficulty of finding enough training data for an input noisy patch directly correlates with diminishing returns in denoising performance. That is, not only is it easier to increase window size for smooth patches, they also benefit more from such an increase. In contrast, textured regions require a significantly larger sample size to increase the patch size, while gaining very little from such an increase. From a practical viewpoint, this analysis suggests an *adaptive strategy* where each pixel is denoised with a variable window size that depends on its local patch complexity.

Next, we put computational issues aside, and study the fundamental limit of denoising, with an infinite window size and a perfectly known $p(x)$ (i.e., an infinite training database). Under a simplified image formation model we study the following question: What is the absolute lower bound on denoising error, and how fast do we converge to it, as a function of window size. We show that the *scale invariance* of natural images plays a key role and yields a power law convergence curve. Remarkably, despite the model's simplicity, its predictions agree well with empirical observations. Extrapolating this parametric law provides a ballpark prediction on the best possible denoising, suggesting that current algorithms may still be improved by about $0.5 - 1$ dB.

2 Optimal Mean Square Error Denoising

In image denoising, given a noisy version $y = x + n$ of a clean image x, corrupted by additive noise n, the aim is to estimate a cleaner version $\hat{x}$. The common quality measure of denoising algorithms is their mean squared error, averaged over all possible clean and noisy x, y pairs, where x is sampled from the density $p(x)$ of natural images

$$\text{MSE} = \mathbb{E}[\|\hat{x} - x\|^2] = \int p(x) \int p(y|x)\|x - \hat{x}\|^2 dy dx \tag{1}$$

It is known, e.g. [14], that for a single pixel of interest x_c the estimator minimizing Eq. (1) is the conditional mean:

$$\hat{x}_c = \mu(y) = \mathbb{E}[x_c|y] = \int \frac{p(y|x)}{p(y)} p(x) x_c dx. \tag{2}$$

Inserting Eq. (2) into Eq. (1) yields that the minimum mean squared error (MMSE) per pixel is the conditional variance

$$\text{MMSE} = \mathbb{E}_y[\mathbb{V}[x_c|y]] = \int p(y) \int p(x|y) \left(x_c - \mu(y)\right)^2 dxdy. \tag{3}$$

The MMSE measures the *inherent ambiguity* of the denoising problem and the statistics of natural images, as any natural image x within the noise level of y may have generated y. Since Eq. (2) depends on the exact unknown density $p(x)$ of natural images (with full image support), it is unfortunately not possible to compute. Nonetheless, by definition it is the theoretically optimal denoising algorithm, and in particular outperforms all other algorithms, even those that detect the class of a picture and then use class-specific priors [3], or those which leverage internal patch repetition [5,25]. That said, such approaches can yield significant practical benefits when using a finite data.

Finally, note that the density $p(x)$ plays a *dual* role. According to Eq. (1), it is needed for evaluating *any* denoising algorithm, since the MSE is the average over natural images. Additionally, it determines the optimal estimator $\mu(y)$ in Eq. (2).

Finite support: First, we consider algorithms that only use information in a window of d noisy pixels around the pixel to be denoised. When needed, we denote by x_{w_d}, y_{w_d} the restriction of the clean and noisy images to a d-pixel window and by x_c, y_c the pixel of interest, usually the central one with $c = 1$. As in Eq. (3), the optimal MMSE_d of any denoising algorithm restricted to a d pixels support is also the conditional variance, but computed over the space of natural patches of size d rather than on full-size images.

By definition, the optimal denoising error may only decrease with window size d, since the best algorithm seeing $d+1$ pixels can ignore the last pixel and provide the answer of the d pixels algorithm. This raises two critical questions: *how does MMSE_d decrease with d, and what is MMSE_∞, namely the best achievable denoising error of* **any** *algorithm (not necessarily patch based) ?*

Non-Parametric approach with a finite training set: The challenge in evaluating MMSE_d is that the density $p(x)$ of natural images is unknown. To bypass it, a non-parametric study of MMSE_d for small values of d was made in [14], by approximating Eq. (2) with a discrete sum over a large dataset of clean d-dimensional patches $\{x_i\}_{i=1}^N$.

$$\hat{\mu}_d(y) = \frac{\frac{1}{N}\sum_i p(y_{w_d}|x_{i,w_d}) x_{i,c}}{\frac{1}{N}\sum_i p(y_{w_d}|x_{i,w_d})} \tag{4}$$

where, for iid zero-mean additive Gaussian noise n with variance σ^2,

$$p(y_{w_d}|x_{w_d}) = \frac{1}{(2\pi\sigma^2)^{d/2}} e^{-\frac{\|x_{w_d} - y_{w_d}\|^2}{2\sigma^2}}. \tag{5}$$

An interesting conclusion of [14] was that for small patches or high noise levels, existing denoising algorithms are close to the optimal MMSE_d.

For Eq. (4) to be an accurate estimate of $\mu_d(y)$, the given dataset must contain many clean patches at distance $(d\sigma^2)^{1/2}$ from y_{w_d}, which is the expected distance between the original and noisy patches, $\mathbb{E}[\|x_{w_d} - y_{w_d}\|^2] = d\sigma^2$. As a result, non-parametric denoising requires a larger training set at low noise levels σ where the distance $d\sigma^2$ is smaller, or at larger patch sizes d where clean patch samples are spread further apart. This curse of dimensionality restricted [14] to small values of d.

In contrast, in this paper we are interested in the best achievable denoising of *any* algorithm, without restrictions on support size, namely MMSE_∞. We thus generalize [14] by studying how MMSE_d decreases as a function of d, and as a result provide a novel prediction of MMSE_∞ (see Section 4).

Note that MMSE_∞ corresponds to an infinite database of all clean images, which in particular also includes the original image x. However, this does not imply that $\text{MMSE}_\infty = 0$, since this database also includes many slight variants of x, with small spatial shifts or illumination changes. Any of these variants may have generated the noisy image y, making it is impossible to identify the correct one with zero error.

3 Patch Size, Complexity and PSNR Gain

Increasing the window size provides a more accurate prior as it considers the information of distant pixels on the pixel of interest. However, in a non-parametric approach, this requires a much larger training set and it is unclear how substantial the PSNR gain might be. This section shows that this tradeoff depends on "patch complexity", and presents a *law of diminishing return*: patches that require a large increase in database size also benefit little from a larger window. This gain is governed by the statistical dependency of peripheral pixels and the central one: weakly correlated pixels provide little information while leading to a much larger spread in patch space, and thus require a significantly larger training data.

3.1 Empirical study

To understand the dependence of PSNR on window size, we present an empirical study with $M = 10^4$ clean and noisy pairs $\{(x_j, y_j)\}_{j=1}^M$ and $N = 10^8$ samples taken from the LabelMe dataset, as in [14]. We compute the non-parametric mean (Eq. (4)) at varying window sizes d. For each noisy patch we determine the largest d at which estimation is still reliable by comparing the results with different clean subsets[1].

[1] We divide the N clean samples into 10 groups, compute the non-parametric estimator $\hat{\mu}_d(y_j)$ on each group separately, and check if the variance of these 10 estimators is much smaller than σ^2. For small d, samples are dense enough and all these estimators provide consistent results. For large d, sample density is insufficient, and each estimator gives a very different result.

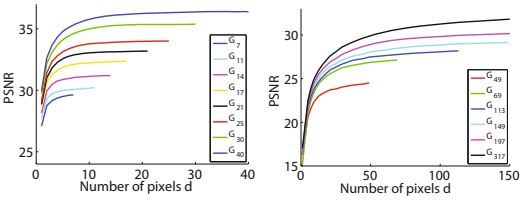

1D signals, $\sigma = 10$ 2D signals, $\sigma = 50$

Fig. 1. For patch groups G_ℓ of varying complexity, we present PSNR vs. number of pixels d in window w_d, where $d = 1, \ldots, \ell$. Higher curves correspond to smooth regions, which flatten at larger patch dimensions. Textured regions correspond to lower curves which not only run out of samples sooner, but also their curves flatten earlier.

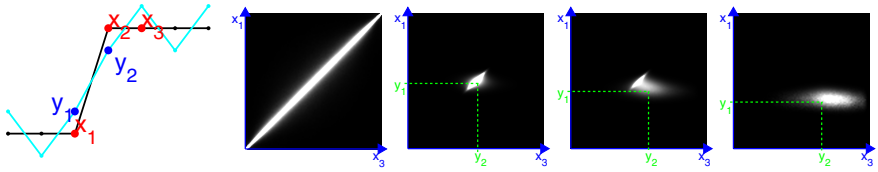

(a) unconditional (b) $|y_1 - y_2| = 10$ (c) $|y_1 - y_2| = 40$ (d) $|y_1 - y_2| = 80$ (e)

Fig. 2. (a) A clean and noisy 1D signal. (b) Unconditional joint distribution $p(x_1, x_3)$. (c-e) Conditional distributions $p(x_1, x_3|y_1, y_2)$ for a few observed gradients $|y_1 - y_2|$, at noise s.t.d. $\sigma = 10$. The original dependence of x_1, x_3 is broken if a high gradient is observed, $|y_1 - y_2| \gg \sigma$.

We divide the M test patches into groups G_ℓ based on the largest window size ℓ at which the estimate is still reliable. For each group, Fig. 1 displays the empirical PSNR averaged over the group's patches as a function of window size d, for $d = 1, \ldots, \ell$ (that is, up to the maximal window size $d = \ell$ at which estimation is reliable), where:

$$\text{PSNR}(G_\ell|w_d) = -10 \log_{10} \left(\frac{1}{|G_\ell|} \sum_{j \in G_\ell} (x_{j,c} - \hat{\mu}_d(y_j))^2 \right)$$

We further compute for each group its mean gradient magnitude, $\|\nabla y_{w_\ell}\|$, and observe that groups with smaller support size ℓ, which run more quickly out of training data, include mostly patches with large gradients (texture). These patches correspond to PSNR curves that are lower and also flatten earlier (Fig. 1). In contrast, smoother patches are in groups that run out of examples later (higher ℓ) and also gain more from an increase in patch width: the higher curves in Fig. 1 flatten later. The data in Fig. 1 demonstrates an important principle: *When an increase in patch width requires many more training samples, the performance gain due to these additional samples is relatively small.*

To understand the relation between patch complexity, denoising gain, and required number of samples, we show that the statistical dependency between adjacent pixels is broken when large gradients are observed. We sample rows of 3 consecutive pixels from clean x and noisy y natural images (Fig. 2(a)), discretize them into 100 intensity

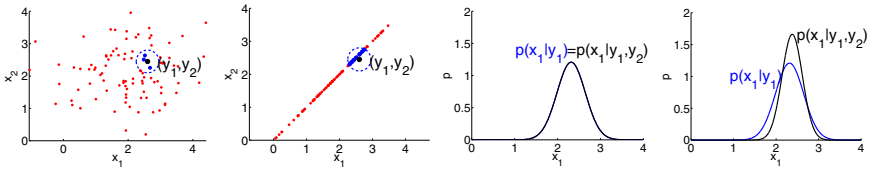

(a) Independent (b) Fully Dependent (c) Independent (d) Fully Dependent
Samples from joint distributions Conditional distributions

Fig. 3. A toy example of 2D sample densities

bins, and estimate the conditional probability $p(x_1, x_3|y_1, y_2)$ by counting occurrences in each bin. When the gradient $|y_2 - y_1|$ is high with respect to the noise level, x_1, x_3 are approximately independent, $p(x_1 = i, x_3 = j||y_1 - y_2| \gg \sigma) \approx p_1(i)p_3(j)$, see Fig. 2(e). In contrast, small gradients don't break the dependency, and we observe a much more elongated structure, see Fig. 2(c,d) . For reference, Fig. 2(b) shows the unconditional joint distribution $p(x_1, x_3)$, without seeing any y. Its diagonal structure implies that while the pixels (x_1, x_3) are by default dependent, the dependency is broken in the presence of a strong edge between them. From a practical perspective, if $|y_1 - y_2| \gg \sigma$, adding the pixel y_3 does not contribute much to the estimation of x_1. If the gradient $|y_1 - y_2|$ is small there is still dependency between x_3 and x_1, so adding y_3 does further reduce the reconstruction error. A simple explanation for this phenomenon is to think of adjacent objects in an image. As objects can have independent colors, the color of one object tells us nothing about its neighbor on the other side of the edge.

3.2 Theoretical Analysis

Motivated by Fig. 1 and Fig. 2, we study the implications of partial statistical dependence between pixels, both on the performance gain expected by increasing the window size, and on the requirements on sample size.

2D Gaussian case: To gain intuition, we first consider a trivial scenario where patch size is increased from 1 to 2 pixels and distributions are Gaussians. In Fig. 3(a), x_1 and x_2 are independent, while in Fig. 3(b) they are fully dependent and $x_1 = x_2$. Both cases have the same marginal distribution $p(x_1)$ with equal denoising performance for a 1-pixel window. We draw $N = 100$ samples from $p(x_1, x_2)$ and see how many of them fall within a radius σ around a noisy observation (y_1, y_2). In the uncorrelated case (Fig. 3(a)), the samples are spread in the 2D plane and therefore only a small portion of them fall near (y_1, y_2). In the second case, since the samples are concentrated in a significantly smaller region (a 1-D line), there are many more samples near (y_1, y_2). Hence, in the fully correlated case a non parametric estimator requires a significantly smaller dataset to have a sufficient number of clean samples in the vicinity of y.

To study the accuracy of restoration, Fig. 3(c,d) shows the conditional distributions $p(x_1|y_1, y_2)$. When x_1, x_2 are independent, increasing window size to take y_2 into account provides no information about x_1, and $p(x_1|y_1) = p(x_1|y_1, y_2)$. Worse, denoising performance decreases when the window size is increased because we now have fewer training patches inside the relevant neighborhood. In contrast, in the fully correlated case, adding y_2 provides valuable information about x_1, and the variance of $p(x_1|y_1, y_2)$ is half of the variance given y_1 alone. This illustrates how high correlation between pixels yields a significant decrease in error without requiring a large increase in sample size. Conversely, weak correlation gives only limited gain while requiring a large increase in training data.

General derivation: We extend our 2D analysis to d dimensions. The following claim, proved in [15], provides the leading error term of the non-parametric estimator $\hat{\mu}_d(y)$ of Eq.(4) as a function of training set size N and window size d. It is similar to results in the statistics literature on the MSE of the Nadaraya-Watson estimator.

Claim. Asymptotically, as $N \to \infty$, the expected non-parametric MSE with a window of size d pixels is

$$\mathbb{E}_N[MSE_d(y)] = MMSE_d(y) + \tfrac{1}{N}\mathcal{V}_d(y) + o\left(\tfrac{1}{N}\right) \tag{6}$$

$$\mathcal{V}_d \approx \frac{\mathbb{V}[x_1|y_{w_d}]\,|\Phi_d|}{\sigma^{2d}}, \tag{7}$$

with $\mathbb{V}[x_1|y_{w_d}]$ the conditional variance of the central pixel x_1 given a window w_d from y, and $|\Phi_d|$ is the determinant of the local $d \times d$ covariance matrix of $p(y)$,

$$|\Phi_d|^{-1} = \left| -\frac{\partial^2 \log p(y_{w_d})}{\partial^2 y_{w_d}} \right|. \tag{8}$$

The expected error is the sum of the fundamental limit $\text{MMSE}_d(y)$ and a variance term that accounts for the finite number of samples N in the dataset. As in Monte-Carlo sampling, it decreases as $\frac{1}{N}$. When window size increases, $\text{MMSE}_d(y)$ decreases, but the variance $\mathcal{V}_d(y)$ might increase. The tension between these two terms determines whether for a constant training size N increasing window size is beneficial.

The variance $\mathcal{V}_d$ is proportional to the volume of $p(y_{w_d})$, as measured by the determinant $|\Phi_d|$ of the local covariance matrix. When the volume of the distribution is larger, the N samples are spread over a wider area and there are fewer clean patches near each noisy patch y. This is precisely the difference between Fig. 3(a) and Fig. 3(b).

For the error to be close to the optimal MMSE_d, the term $\mathcal{V}_d/N$ in Eq. (6) must be small. Eq. (7) shows that $\mathcal{V}_d$ depends on the volume $|\Phi_d|$ and we expect this term to grow with dimension d, thus requiring many more samples N. Both our empirical data and our 2D analysis show that the required increase in sample size is a function of the statistical dependency of the central pixel with the added one.

To understand the required increase in training size N when window size is increased by one pixel from $d-1$ to d, we analyze the ratio of variances $\mathcal{V}_d/\mathcal{V}_{d-1}$. Let $g_d(y)$ be the gain in performance (for an infinite dataset), which according to Eq. (3) is given by:

$$g_d(y) = \frac{\text{MMSE}_{d-1}(y)}{\text{MMSE}_d(y)} = \frac{\mathbb{V}[x_1|y_1, \dots y_{d-1}]}{\mathbb{V}[x_1|y_1, \dots y_d]} \tag{9}$$

We also denote by $g_d^*(y)$ the ideal gain if x_d and x_1 were perfectly correlated, i.e. $r = cor(x_1, x_d \,|\, y_1, \dots, y_{d-1}) = 1$. Assuming for simplicity a Gaussian distribution, the following claim shows that when $\text{MMSE}_d(y)$ is most improved, sampling is not harder since the volume and variance $\mathcal{V}_d$ do not grow.

Claim. Let $p(y)$ be Gaussian. When increasing the patch size from $d-1$ to d, the variance ratio and the performance gain of the estimators are related by:

$$\frac{\mathcal{V}_d}{\mathcal{V}_{d-1}} = \frac{g_d^*}{g_d} \geq 1. \tag{10}$$

That is, the ratio of variances equals the ratio of optimal denoising gain to the achievable gain. When x_1, x_d are perfectly correlated, $g_d = g_d^*$, we get $\mathcal{V}_d/\mathcal{V}_{d-1} = 1$, and a larger window gives improved restoration results without increasing the required dataset size. In contrast, if x_d, x_1 are weakly correlated, increasing window size requires a bigger dataset to keep $\mathcal{V}_d/N$ small, and yet the PSNR gain is small.

Proof. Let C be the 2×2 covariance of x_1, x_d given $y_1, \dots, y_{d-1}$ (before seeing y_d)

$$C = Cov(x_1, x_d|y_1, \dots y_{d-1}) = \begin{pmatrix} c_1 & c_{12} \\ c_{12} & c_2 \end{pmatrix} \tag{11}$$

and let $r = c_{12}/\sqrt{c_1 c_2}$ be the correlation between x_1, x_d.

Under the Gaussian assumption, upon observing y_d, the marginal variance of x_1 decreases from c_1 to the following expression (see Eq. 2.73 in [4]),

$$\mathbb{V}[x_1|y_1, \dots, y_d] = c_1 - \frac{c_{12}^2}{c_2 + \sigma} = c_1 \left(1 - \frac{c_{12}^2/c_1}{c_2 + \sigma^2}\right) = c_1 \frac{c_2(1-r^2) + \sigma^2}{c_2 + \sigma^2}. \tag{12}$$

Hence the contribution to performance gain of the additional pixel y_d is

$$g_d = \frac{\mathbb{V}[x_1|y_1, \dots y_{d-1}]}{\mathbb{V}[x_1|y_1, \dots y_d]} = \frac{c_2 + \sigma^2}{c_2(1-r^2) + \sigma^2}. \tag{13}$$

When $r = 1$, the largest possible gain from y_d is $g_d^* = (c_2 + \sigma^2)/\sigma^2$. The ratio of best possible gain to achieved gain is

$$\frac{g_d^*}{g_d} = \frac{c_2(1-r^2) + \sigma^2}{\sigma^2}. \tag{14}$$

Next, let us compute the ratio $\mathcal{V}_d/\mathcal{V}_{d-1}$. For Gaussian distributions, according to Eq. 2.82 in [4], the conditional variance of y_d given $y_1, \dots, y_{d-1}$ is independent of the specific observed values. Further, since $p(y_1, \dots, y_d) = p(y_1, \dots, y_{d-1})p(y_d|y_1, \dots y_{d-1})$, we obtain that

$$|\Phi_d| = \mathbb{V}(y_d|y_1, \dots y_{d-1})|\Phi_{d-1}| \tag{15}$$

Table 1. Adaptive and fixed window denoising results in PSNR

σ	20	35	50	75	100
Optimal Fixed	32.4	30.1	28.7	27.2	26.0
Adaptive	33.0	**30.5**	**29.0**	**27.5**	**26.4**
BM3D	**33.2**	30.3	28.6	26.9	25.6

This implies that

$$\frac{\mathcal{V}_d}{\mathcal{V}_{d-1}} = \frac{\mathbb{V}(y_d|y_1,\dots y_{d-1})}{\sigma^2}\frac{\mathbb{V}[x_1|y_1,\dots y_d]}{\mathbb{V}[x_1|y_1,\dots y_{d-1}]} \tag{16}$$

Next, since $y_d = x_d + n_d$ with $n_d \sim N(0,\sigma^2)$ independent of $y_1,\dots,y_{d-1}$, then $\mathbb{V}(y_d|y_1,\dots y_{d-1}) = c_2 + \sigma^2$. Thus,

$$\frac{\mathcal{V}_d}{\mathcal{V}_{d-1}} = \frac{c_2+\sigma^2}{\sigma^2}\frac{c_2(1-r^2)+\sigma^2}{c_2+\sigma^2} = \frac{g_d^*}{g_d}.$$

□

In [15] we compute $\mathcal{V}_d$ and g_d for several cases. For a signal whose pixels are all independent with equal variance, $\mathcal{V}_d$ and the required number of samples N both grow exponentially with dimension d. In contrast, for a fully correlated signal, $\mathcal{V}_d$ is constant.

3.3 Adaptive Denoising

Our analysis suggests that patch based denoising can be improved mostly in flat areas and less in textured ones. In [15] we show that this is implicit in several recent works, consistent with [7]. This motivates an *adaptive* denoising scheme [12] where each pixel is denoised with a variable patch size that depends on its local image complexity. To test this idea, we devised the following scheme. Given a noisy image, we denoise each pixel using several patch widths and multiple disjoint clean samples. As before, we compute the variance of all these different estimates, and select the largest width for which the variance is still below a threshold. Table 1 compares the PSNR of this adaptive scheme to fixed window size non-parametric denoising using the optimal window size at each noise level, and to BM3D [8], a state-of-the-art algorithm. We used $M = 1000$ test pixels and $N = 7 \cdot 10^9$ clean samples. At all considered noise levels, the adaptive approach significantly improves the fixed patch approach, by about $0.3 - 0.6$dB. At low noise levels, sample size N is too small, and adaptive denoising is worse than BM3D[2]. At higher noise levels it increasingly outperforms BM3D.

Fig. 4 visualizes the difference between the adaptive and fixed patch size approaches, at noise level $\sigma = 50$. When patch size is small, noise residuals are highly visible in

[2] The reason is that at this finite N, with $\sigma = 20$ our non-parametric approach uses 5×5 patches at textured regions. In contrast, BM3D uses 8×8 ones, with additional algorithmic operations which allow it to better generalize from a limited number of samples.

(a)Original (b)Noisy input (c)Adaptive (d)Fixed $k = 5$ (e)Fixed $k = 6$ (f)Fixed $k = 10$

Fig. 4. Visual comparison of adaptive vs. fixed patch size non parametric denoising (optimal fixed size results obtained with $k = 6$). A fixed patch has noise residuals either in flat areas(d,e), or in textured areas(f).

the flat regions. With a large patch size, one cannot find good matches in the textured regions, and as a result noise is visible around edges. Both edges and flat regions are handled properly by the adaptive approach. Moreover, under perceptual error metrics such as SSIM [24], decreasing the error in the smooth regions is more important, thus underscoring the potential benefits of an adaptive approach.

Note that this adaptive non-parametric denoising is not a practical algorithm, as Fig. 4 required several days of computation. Nonetheless, these results suggest that adaptive versions to existing denoising algorithms such as [10,8,16,9,26] and other low-level vision tasks are a promising direction for future research.

4 The Convergence and Limits of Optimal Denoising

In this section, we put computational and database size issues aside, and study the behavior of optimal denoising error as window size increases to infinity. Fig. 1 shows that optimal denoising yields a diminishing return beyond a window size that varies with patches. Moreover, patches that plateau at larger window sizes also reach a higher PSNR. Fig. 2 shows that strong edges break statistical correlation between pixels. Combining the two suggests that each image pixel has a finite compact region of informative neighboring pixels. Intuitively, the size distribution of these regions must directly impact both denoising error vs. window size and its limit with an infinite window.

We make two contributions towards elucidating this question. First we show that a combination of the simplified *dead leaves* image formation model, together with *scale invariance* of natural images implies both a *power-law* convergence, $\text{MMSE}_d \sim e + c/d$, as well as a strictly positive lower bound on the optimal denoising with infinite window, $\text{MMSE}_\infty = e > 0$. Next, we present empirical results showing that despite the simplicity of this model, its conclusions match well the behavior of real images.

4.1 Scale-Invariance and Denoising Convergence

We consider a *dead leaves* image formation model, e.g. [1], whereby an image is a random collection of piecewise constant segments, whose size is drawn from a scale-invariant distribution and whose intensity is drawn i.i.d. from a uniform distribution. This yields perfect correlation between pixels in the same region, as in Fig. 3(b).

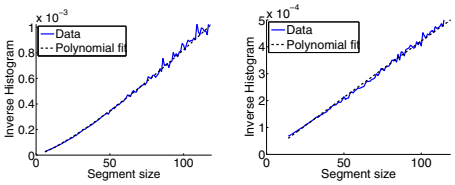

$T = 5, h(d) \propto d^{-1.2}$ $T = 20, h(d) \propto d^{-1}$

Fig. 5. Inverse histograms of segment lengths follow a scale invariant distribution

To further simplify the analysis, we conservatively assume an edge oracle which gives the exact locations of edges in the image. The optimal denoising is then to average all observations in a segment. For a pixel belonging to segment of size s pixels, the MMSE is σ^2/s. Overall the expected reconstruction error with infinite-sized windows is

$$\text{MMSE} = \int p(s)\frac{\sigma^2}{s}ds \tag{17}$$

where $p(s)$ is the probability that a pixel belongs to a segment with s pixels. The optimal error is strictly larger than zero if the probability of finite segments is larger than zero. Without the edge-oracle, the error is even higher.

Scale Invariance: Scale invariance is a fundamental property of natural images. As shown in numerous studies, down-sampling natural images retains many of their statistical properties, from gradient distributions to segment (region) areas, e.g. [11,23,1,17,21]. A simple argument [1,15] shows that scale-invariance implies that the probability that a random image pixel belongs to a segment of size s is of the form $p(s) \propto 1/s$. In a Markov model, in contrast, $p(s)$ decays exponentially fast with s [21,15].

To get a sense of the empirical size distribution of nearly-constant-intensity regions in natural images, we perform a simple experiment inspired by [1]. For a random set of pixels $\{x_i\}$, we compute the size $d(i)$ of the connected region whose pixel values differ from x_i by at most a threshold T: $d(i) = \#\{x_j || x_j - x_i| \leq T\}$. The empirical histogram $h(d)$ of region sizes follows a power law behavior $h(d) \propto d^{-\alpha}$ with $\alpha \approx 1$, as shown in Fig. 5(a,b), which plots $1/h(d)$.

Optimal denoising as a function of window size: We now compute the optimal denoising for the dead leaves model with the scale invariance property. Since $1/s$ is not integrable, scale invariance cannot hold at infinitely large scales. Assuming it holds up to a maximal size $D \gg 1$, gives the normalized probability

$$p_D(s) = \frac{s^{-1}}{\int_1^D s^{-1}ds} = \frac{1}{\ln D}\frac{1}{s}. \tag{18}$$

We compute the optimal error with a window of size $d \ll D$ pixels. Given the edge oracle, every segment of size $s \leq d$ attains its optimal denoising error of σ^2/s, whereas

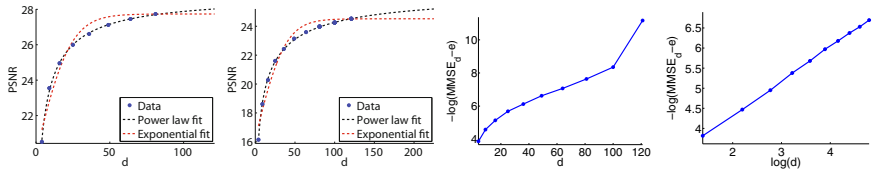

(a) $\sigma = 50$ (b) $\sigma = 100$ (c) Log plot (d) Log log plot

Fig. 6. PSNR vs. patch dimension. A power law fits the data well, whereas an exponential law fits poorly. Panels (c) and (d) show $|\log(\text{MMSE}_d - e)|$ v.s. d or $\log(d)$. An exponential law should be linear in the first plot, a power law linear in the second.

if $s > d$ we obtain only σ^2/d. Splitting the integral in (17) into these two cases gives

$$\begin{aligned}\text{MMSE}_d &= \int_1^d \frac{\sigma^2}{s} p_D(s) ds + \int_d^D \frac{\sigma^2}{d} p_D(s) ds \qquad (19)\\ &= \text{MMSE}_D + \frac{\sigma^2}{d}\left(1 - \frac{\ln d + 1}{\ln D}\right) + \frac{\sigma^2}{D \ln D} \approx \text{MMSE}_D + \frac{\sigma^2}{d}\end{aligned}$$

For this model, $\text{MMSE}_\infty = \text{MMSE}_D$. Thus, *the dead leaves model with scale invariance property implies a power law* $1/d$ *convergence to a strictly positive MMSE*$_\infty$.

4.2 Empirical Validation and Optimal PSNR

While dead leaves is clearly an over-simplified model, it captures the salient properties of natural images. Even though real images are not made of piecewise constant segments, the results of Sec. 3, and Fig. 5 suggest that each image pixel has a finite "informative region", whose pixel values are most relevant for denoising it. While for real images, correlations may not be perfect inside this region and might not fully drop to zero outside it, we now show that empirically, optimal denoising in natural images indeed follows a power law similar to that of the dead-leaves model.

To this end, we apply the method of [14] and compute the optimal patch based MMSE_d for several small window sizes d. Fig. 6(a-b) show that consistent with the dead leaves model, we obtain an excellent fit to a power law $\text{MMSE}_d = e + \frac{c}{d^\alpha}$ with $\alpha \approx 1$. In contrast, we get a poor fit to an exponential law, $\text{MMSE}_d = e + cr^{-d}$, implied by the common Markovian assumption [21,15]. In addition, Fig. 6(c,d) show log and log-log plots of $(\text{MMSE}_d - e)$, with the best fitted e in each case. The linear behavior in the log-log plot (Fig. 6(d)) further supports the power law. Fitting details appear in [15].

Predicting Optimal PSNR: For small window sizes, using a large database and Eq. (4), we can estimate the optimal patch-based denoising MMSE_d. Fig. 6 shows that the curve of MMSE_d is accurately fitted by a power law $\text{MMSE}_d = e + c/d^\alpha$, with $\alpha \approx 1$. Extrapolating this curve, we can predict the value of MMSE_∞, which is the best possible error of *any* denoising algorithm (not necessarily patch based). Since the power law is only approximate, this extrapolation should be taken with a grain of salt. Nonetheless,

Table 2. Extrapolated optimal denoising in PSNR, and the results of recent algorithms. A modest room for improvement exists.

σ	35	50	75	100
Extrapolated bound (PSNR_∞)	30.6	28.8	27.3	26.3
KSVD [10]	28.7	26.9	25.0	23.7
BM3D [8]	30.0	28.1	26.3	25.0
EPLL [26]	29.8	28.1	26.3	25.1

it gives an interesting ballpark estimate on the amount of further achievable gain by any future algorithmic improvements. Table 2 compares the PSNR of existing algorithms to the predicted PSNR_∞, over $M = 20,000$ patches using the power law fit based on $N = 10^8$ clean samples[3]. The comparison suggests that depending on noise level σ, current methods may still be improved by $0.5 - 1$dB. While the extrapolated value may not be exact, our analysis does suggest that there are inherent limits imposed by the statistics of natural images, which cannot be broken, no matter how sophisticated future denoising algorithms will be.

5 Discussion

In this paper we studied both computational and information aspects of image denoising. Our analysis revealed an intimate relation between denoising performance and the scale invariance of natural image statistics. Yet, only few approaches account for it [20]. Our findings suggest that scale invariance can be an important cue to explore in the development of future natural image priors. In addition, adaptive patch size approaches are a promising direction to improve current algorithms, such as [10,8,16,9,26].

Our work also highlights the relation between the frequency of occurrence of a patch, local pixel correlations, and potential denoising gains. This concept is not restricted to the denoising problem, and may have implications in other fields.

Acknowladgments. We thank ISF, BSF, ERC, Intel, Quanta and NSF for funding.

References

1. Alvarez, L., Gousseau, Y., Morel, J.: The size of objects in natural images (1999)
2. Arietta, S., Lawrence, J.: Building and using a database of one trillion natural-image patches. In: IEEE Computer Graphics and Applications (2011)
3. Baker, S., Kanade, T.: Limits on super-resolution and how to break them. PAMI (2002)
4. Bishop, C.M.: Pattern recognition and machine learning. Springer (2006)
5. Buades, A., Coll, B., Morel, J.: A review of image denoising methods, with a new one. Multiscale Model. Simul. (2005)

[3] The numerical results in Tables 1,2 are not directly comparable, since Table 1 was computed on a small subset of only $M = 1,000$ test examples, but with a larger sample size N.

6. Chandler, D., Field, D.: Estimates of the information content and dimensionality of natural scenes from proximity distributions. J. Opt. Soc. Am. (2007)
7. Chatterjee, P., Milanfar, P.: Is denoising dead? IEEE Trans. Image Processing (2010)
8. Dabov, K., Foi, A., Katkovnik, V., Egiazarian, K.: Image denoising by sparse 3-d transform-domain collaborative filtering. IEEE Trans. Image Processing (2007)
9. Dong, W., Li, X., Zhang, L., Shi, G.: Sparsity-based image denoising vis dictionary learning and structural clustering. In: CVPR (2011)
10. Elad, M., Aharon, M.: Image denoising via sparse and redundant representations over learned dictionaries. IEEE Trans. Image Processing (2006)
11. Field, D.: Relations between the statistics of natural images and the response properties of cortical cells. In: JOSA (1978)
12. Kervrann, C., Boulanger, J.: Optimal spatial adaptation for patch-based image denoising. In: ITIP (2006)
13. Lee, A., Pedersen, K., Mumford, D.: The nonlinear statistics of high-contrast patches in natural images. In: IJCV (2003)
14. Levin, A., Nadler, B.: Natural image denoising: optimality and inherent bounds. In: CVPR (2011)
15. Levin, A., Nadler, B., Durand, F., Freeman, W.: Patch complexity, finite pixel correlations and optimal denoising. Technical report, MIT CSAIL TR 2012-022
16. Mairal, J., Bach, F., Ponce, J., Sapiro, G., Zisserman, A.: Non-local sparse models for image restoration. In: ICCV (2009)
17. Mumford, D., Gidas, B.: Stochastic models for generic images. Quarterly of Applied Mathematics (2001)
18. Osindero, S., Hinton, G.: Modeling image patches with a directed hierarchy of markov random fields. In: NIPS (2007)
19. Polzehl, J., Spokoiny, V.: Image denoising: Pointwise adaptive approach. Annals of Statistics 31, 30–57 (2003)
20. Portilla, J., Strela, V., Wainwright, M., Simoncelli, E.: Image denoising using scale mixtures of gaussians in the wavelet domain. IEEE Trans. Image Processing (2003)
21. Ren, X., Malik, J.: A Probabilistic Multi-scale Model for Contour Completion Based on Image Statistics. In: Heyden, A., Sparr, G., Nielsen, M., Johansen, P. (eds.) ECCV 2002, Part I. LNCS, vol. 2350, pp. 312–327. Springer, Heidelberg (2002)
22. Roth, S., Black, M.J.: Fields of experts: A framework for learning image priors. In: CVPR (2005)
23. Ruderman, D.: Origins of scaling in natural images. Vision Research (1997)
24. Wang, Z., Bovik, A.C., Sheikh, H.R., Simoncelli, E.P.: Image quality assessment: From error visibility to structural similarity. IEEE Trans. on Image Processing (2004)
25. Zontak, M., Irani, M.: Internal statistics of a single natural image. In: CVPR (2011)
26. Zoran, D., Weiss, Y.: From learning models of natural image patches to whole image restoration. In: ICCV (2011)